Astron. Astrophys. 332, 165–172 (1998)

ASTRONOMY AND ASTROPHYSICS

The SIGMA pulse profiles of GX 1+4: four years of monitoring

P. David[1], P. Laurent[1], M. Denis[2], J. Paul[1] L. Bouchet[3], J.-P. Roques[3], E. Jourdain[3], G. Vedrenne[3], M. Gilfanov[4], M. Churazov[4], R.A. Sunyaev[4], N. Khavenson[4], B. Novikov[4], I. Chulkov[4], and A. Kuznetzov[4]

[1] Service d'Astrophysique, DAPNIA/DSM/CEA, Centre d'Etudes de Saclay, F-91191 Gif-sur-Yvette, France
[2] Space Research Centre–Polish Academy of Sciences, Bartycka 18A, PL-00716 Warsaw, Poland
[3] Centre d'Etudes Spatiale des Rayonnements, 9 avenue du Colonel Roche, BP 4346, F-31029 Toulouse Cedex, France
[4] Space Research Institute, Russian Academy of Sciences, Profsoyuznaya 84/32, 117810 Moscow, Russia

Received 30 July 1997 / Accepted 11 December 1997

Abstract. The soft γ–ray source GX 1+4 has been regularly monitored by the SIGMA telescope on board GRANAT since 1990. The accumulated data provides both period and spectral information on this source in the 35–150 keV range. The SIGMA telescope also allows a determination of a pulsed fraction. We report here on the last six years of the SIGMA data on GX 1+4. The general spin down trend is confirmed and the derived periods are consistent with those obtained at other energies. The pulse profiles are shown to be roughly divided into two groups. One including those instances when GX 1+4 presents a relatively high pulsed fraction ($> 50\%$), the other containing those when the source exhibits a low pulsed fraction ($< 50\%$). In an effort to understand this result, we construct an emission model which is based nearly entirely on the geometry of the system to describe the pulse profiles. It is found that the pulsed fraction might possibly be linked to the height of the accretion column.

Key words: X-rays: stars – individual: GX 1+4 – gamma-rays: observations

1. Introduction

The galactic centre hard X–ray pulsar GX 1+4 was first detected in a balloon experiment by Lewin et al. (1971) with a pulse period of 135 s. The companion of GX 1+4, the symbiotic M6III giant (V2116 Oph), was identified by Davidsen et al. (1976, 1977). At the time of its discovery, GX 1+4 was the hardest X–ray binary pulsar known and one of the brightest sources in the Galaxy with a luminosity 10^{37}–10^{38} assuming a distance of 8.5 kpc. Subsequent observations revealed the source to be in very fast spin up phase. In the early 80's, however, GX 1+4 disappeared from view, entering into a low luminosity state. Attempts to detect the source with EXOSAT in 1983 and 1984 failed down to an upper limit of 0.4m Crab (Mukai 1988). It was not until 1983 that the source was again weakly detected by GINGA at 3 mCrab (Makishima et al. 1988). Further observations revealed GX 1+4 to be increasing in luminosity and unambiguously showed that the pulsar had undergone a torque reversal, spinning down at a steady rate of ~ 1.4 s yr^{-1}. This spin down episode and relatively low luminosity state has continued up to the present date.

From the onset of its operation, the SIGMA telescope has devoted a large part of its observational time to the monitoring of the Galactic centre. Thus, over a span of six years, GX 1+4 has been sighted in the 35–150 keV energy range numerous times. The data collected in 1990 and 1991 has been analysed and discussed by Barret et al. (1991) and Laurent et al. (1993). In this paper we concentrate on the period covering 1992 to 1996, and more precisely we attempt to obtain more information on the geometric configuration of GX 1+4 based on the study of the pulse profiles which could be extracted. In order to perform such a study, a model of the accreting neutron star is constructed based on simple geometric considerations. Our desire is to be able to describe the shape of the pulse profiles without recourse to ad hoc assumptions on the local emission patterns at the poles of the neutron star since this can not be retrieved from the data in a trivial way. We thus digress from the usual method of pulse profile analysis.

The study of the profiles permit a determination of the inclination between the magnetic and rotational axis. Our model allows an estimation of the vertical dimensions of the accretion funnel which we tentatively link to observed variations in the pulsed fractions. It can also provide insight into the physical processes which occur near the surface of the neutron star but this is beyond the scope of the present paper.

2. Observations and data reduction

The Galactic centre has been regularly monitored by the SIGMA telescope on board GRANAT since 1990 (see Paul et al. 1991 for a description of the instrument). Observations of this region were systematically programmed to be performed in spring and

Send offprint requests to: P. David

fall of each year. Typically, an observation consists of three series of images in 95 energy channels along with the total camera count rates binned into 4 s intervals in four energy bands. The SIGMA position of GX 1+4, viz. α_{1950} = 262.26°; δ_{1950} = −24.74° (Laurent et al. 1991), has thus been sighted some 140 times since the inauguration of the GRANAT observatory. For this binary system, the SIGMA data base provides spectra in the 0.035 – 1.3 MeV energy range as well as the pulsation periods over six years.

The observations of concern here, stretching from 1992 February to 1996 March, are listed in Table 1. Note that all the entries in this table are not relative to an unique pointing session of the source, but that some are the sum of two consecutive pointing sessions. The reason for integrating over two observations was to improve the signal to noise ratio (S/N), when possible. However, for the purpose of measuring a pulsation period, the total integration time was limited to a span over which the known period derivative of GX 1+4 ($\dot{P} \sim 2$ s yr^{-1}) would not affect an epoch folding analysis in which a shift term is not included. Thus we imposed that the total observation times, T_{obs}, were such that the spacing between independent periods, $\Delta P = P^2/T_{obs}$, was substantially greater than the expected $\dot{P}$.

Although Table 1 is not an exhaustive list of all the observations of GX 1+4 carried out by SIGMA, pulsation periods were indeed searched for in all the observations using an epoch folding procedure (Leahy et al. 1983) and, all corresponding images were reduced in order to determine a spectrum. Only those observation for which a period determination was effectively possible and/or a spectrum could be extracted from the image data are included in this table. The results of the epoch folding analysis are given in Table 2, periods are within a 90% confidence level. The binned light curves are displayed in Fig. 1.

The observation modes of the SIGMA instruments allow a determination of the pulsed fraction defined as the ratio between the modulated and the modulated plus steady component count rates. The images provide the total flux from the source while the light curves, scaled by a factor of ~ 3 for calibration with the images, independently obtained from the total camera count rates, furnish the pulsed signal. Note that three cases present themselves in the SIGMA data,

1. both a spectrum and a period determination can be obtained from the data,
2. only a period determination is possible, the integrated source luminosity is below the 3σ detection threshold,
3. there is no pulsed signal, but a spectrum could be extracted from the image data.

For case 1, the calculation of the pulsed fraction, F_{mod}/F_{tot}, is straightforward; the spectral images, corrected for spatial non uniformities and deconvolved using standard techniques, specifically implemented for the SIGMA instrument (Goldwurm 1996), were used to determine the total integrated source flux. A one σ estimation of the modulated flux has been assumed for F_{mod} in the second case. Finally in the third case, a power law spectrum with photon index of −3 has been assumed in order to estimate the upper limit to F_{tot} for a 3σ detection level. In this last case, the apparently unique presence of a pulsed signal is likely to be due to the fact that imaging process is ~ 3 times less sensitive thean the timing analysis. When no spectral images could be extracted from the data, the total source count rates were generally lower than about 0.12 cts s^{-1}. The resulting pulsed fractions, in the 40–77 keV energy band, are also resumed in Table 2.

Table 1. Observations of GX 1+4 1992 to 1996

Date (mon yr days)	JD$_m$	Exposure (s)	F_{tot} (cts s^{-1})	S/N
02 92 17.52–19.59	8671	62404.3	0.15	5.32
02 92 21.51–23.53	8675	120760.6	0.12	4.00
03 92 01.71–03.64	8684	113835.7	0.13	4.16
09 93 00.82–02.32	9232	82196.5	< 0.10	
09 93 02.44–03.44	9233	60610.4	< 0.12	
09 93 04.77–06.32	9236	86586.6	0.26	5.41
09 93 06.45–07.92	9238	88119.4	0.21	3.80
09 93 08.77–10.32	9240	81892.4	0.30	5.82
09 93 10.44–12.05	9242	97051.3	0.23	4.14
09 93 12.83–14.32	9244	79962.5	0.27	5.12
09 93 14.45–16.16	9246	100148.7	0.17	4.02
09 93 17.43–19.34	9249	106903.5	< 0.06	
10 93 12.48–14.09	9274	96680.0	0.12	3.57
03 94 01.68–03.14	9414	87940.4	0.18	3.96
09 95 09.53–11.36	9971	100501.5	0.26	4.96
09 95 13.40–15.22	9975	107021.9	0.24	4.07
09 95 16.58–17.78	9978	70999.0	0.30	4.06
09 95 18.42–19.37	9979	56339.5	< 0.12	
03 96 18.92–20.38	10162	85775.5	0.31	4.50
03 96 20.77–22.48	10164	96628.1	0.32	5.46
03 96 23.52–24.52	10167	59008.7	0.32	4.22
03 96 24.77–26.48	10168	99151.9	< 0.14	
03 96 28.79–30.50	10172	92040.0	< 0.14	

Results from the image data in the 40-77 keV energy range. In this paper, the modified Julian date, JD$_m$, is defined as the reduced Julian date minus 40000, i.e. JD$_m$ = Julian date $- 2,440,000.5$.

3. Emission model

Table 2 indicates that the pulsed fraction is not constant. The reasons behind this behaviour of GX 1+4 are not clear, however, a change in the configuration of the accretion geometry is a plausible explanation. Although it has been pointed out by Li & Wang (1992) that changes in the inclination of the magnetic axis might lead to variations in the luminosity of some pulsars, over the time scale of days, it is unlikely that this will occur. Likewise, variations in the angle between the rotation axis and the line of sight does not appear to be responsible for the changes in the pulsed fractions. Indeed no obvious evidence of a precession period is discernible in the data.

The X–ray profiles of pulsars are frequently modelled by assuming that the high energy emission originates in polar caps or rings situated at the magnetic poles of the neutron star. Assuming the inclinations of the magnetic axis and the line of sight

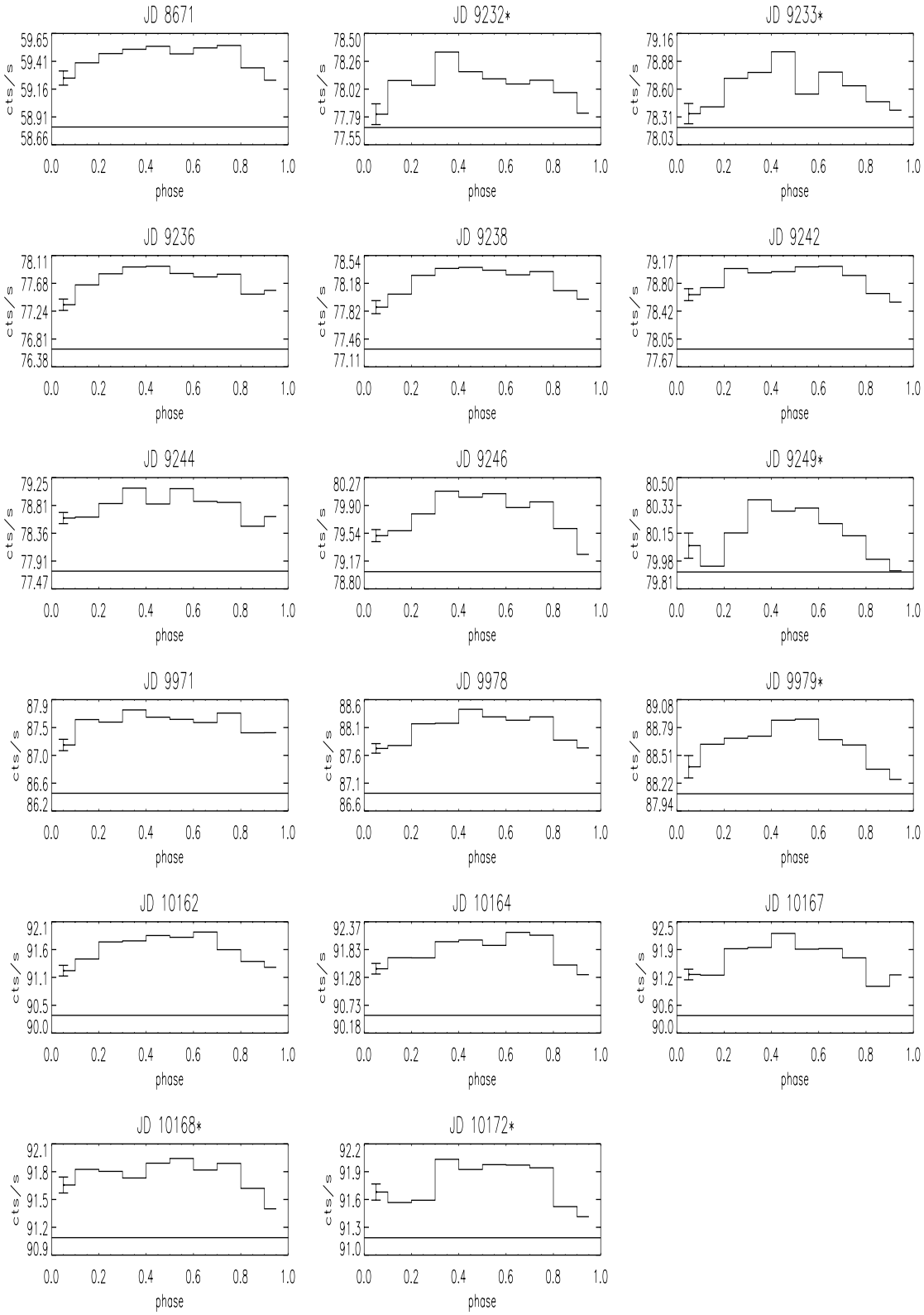

Fig. 1. Pulse profiles of GX 1+4 obtained from 1992 to 1996 by SIGMA in the 40–77 keV energy range. Intensity measured in counts per second versus phase. The profiles have been phase shifted so as to place the maximum in the central bin. The horizontal line represents the background, $(\sup[Y_i] + \inf[Y_i])/2 - S$, where Y_i is the signal obtained from the total camera count rates and, S the flux independently measured from the image data. Dates marked with an asterix (*) are those on which no spectrum was available from the image data.

Table 2. Periods, pulsed fluxes, and pulsed fractions

JD_m	Period (s)	F_{mod} (cts s^{-1})	F_{mod}/F_{tot} (%)	class
8671	117.359 ± 0.016	0.051 ± 0.005	34 ± 7	C_1
8675		< 0.0016	< 2	
8684		< 0.0016	< 5	
9232	120.556 ± 0.024	0.065 ± 0.007	> 58	C_2
9233	120.557 ± 0.028	0.067 ± 0.009	> 49	C_2
9236	120.573 ± 0.015	0.099 ± 0.007	38 ± 8	C_1
9238	120.587 ± 0.015	0.086 ± 0.007	41 ± 11	C_1
9240		< 0.0016	< 2	
9242	120.644 ± 0.015	0.078 ± 0.007	34 ± 9	C_1
9244	120.668 ± 0.020	0.083 ± 0.007	31 ± 7	C_1
9246	120.675 ± 0.008	0.135 ± 0.007	79 ± 20	?
9249	120.708 ± 0.016	0.058 ± 0.007	> 86	C_2
9274		< 0.0016	< 6	
9414		< 0.0016	< 4	
9971	122.877 ± 0.021	0.085 ± 0.007	33 ± 7	C_1
9975		< 0.0016	< 3	
9978	122.923 ± 0.009	0.089 ± 0.007	30 ± 8	C_1
9979	122.942 ± 0.040	0.090 ± 0.009	> 67	C_2
10162	123.778 ± 0.012	0.102 ± 0.008	33 ± 8	C_1
10164	123.802 ± 0.015	0.118 ± 0.009	37 ± 7	C_1
10167	123.806 ± 0.016	0.153 ± 0.009	48 ± 12	?
10168	123.825 ± 0.020	0.100 ± 0.008	> 66	C_2
10172	123.859 ± 0.013	0.091 ± 0.007	> 60	C_2

Results from the folding analysis in the 40–77 keV energy band. For entries where no pulsation was found no period is listed. A lower limit for the pulsed fraction is given when no pulsation was detected. An upper limit is given on those occasions when no spectrum could be extracted from the data (see text). The column, class, refers to the classification of the pulsed fractions described in the text (Sect. 5).

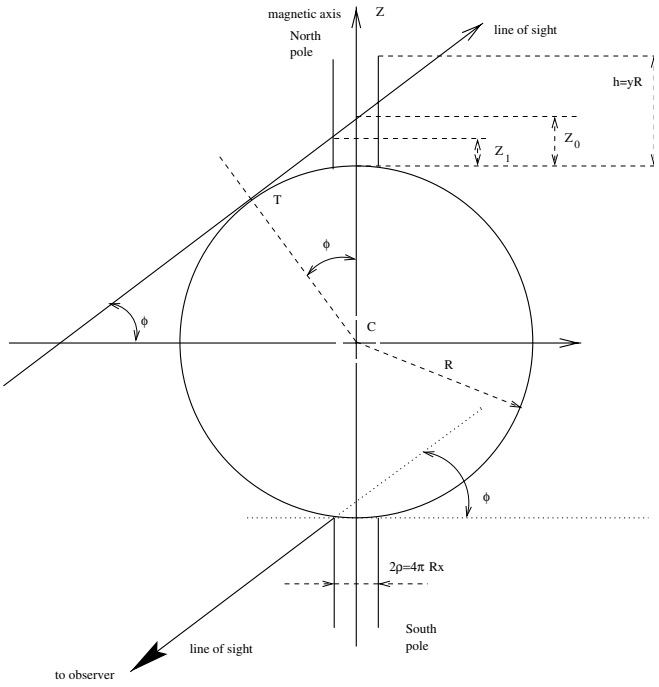

Fig. 2. The geometric configuration of the emitting cylinders on the surface of the neutron star showing the definition of the various parameters used to describe the system.

remain constant over the observation span of concern here, and following the work of Leahy (1990), an attempt was made to determine if the extension of the polar caps could be linked to the variations in the light curves and pulsed fractions. The results of these fits were inconclusive, leaving only the possibility of redefining the beam pattern. In principal, a given beam pattern can be produced by a particular geometry of the emitting region, thus if the beam pattern is known the inverse problem can be solved. This mathematical problem, however, is beyond the scope of the present work. Furthermore, since the SIGMA data does not offer much information on the possible beam patterns, it is preferable to use simpler models rather than introduce ad hoc assumptions which are difficult to check. Moreover, the polar cap/ring models do not easily accommadate the steady emission component observed from GX 1+4, on the other hand, the model described below can account for this.

Our intent here, then, is to limit as much as possible any assumption on the local emission pattern of the emitting regions and to concentrate on a plausible geometry which is capable of reproducing the observed γ–ray light curves of GX 1+4. Following Basko & Sunyaev (1976), the accretion column at the magnetic poles will be modelled by a hollow, thin walled, cylinder of height h and radius ρ. The results of this model are discussed in Sects. 4 and 5.

It is assumed that two cylinders, each positioned at one of the magnetic poles, produce the observed high energy light curves. The only assumptions made on the local emission pattern is that the flux density is uniform over the surface of each of the emitting cylinders, of specific intensity E_0 erg cm^{-2} s^{-1}, and that the high energy flux is emitted isotropically towards the exterior of the emitting cylinder. The model in itself does not restrict each cylinder to have the same specific intensity or equal dimensions.

The axis of both cylinders are taken to coincide with the stellar magnetic axis, see Fig. 2. The magnetic field is assumed to be that of a magnetic dipole. Consequently the entire system is axisymmetric about the stellar magnetic axis, Z. To obtain a more convenient parameterisation of the problem, the dimensionless parameters x and y, defined by $h = Ry$ and $\rho = 2\pi Rx$, where R is the radius of the neutron star, will be introduced.

The line of sight intersects the plane, P, perpendicular to the magnetic axis at an angle ϕ. Choosing a plane, P', that intersects P at the same angle, the intersection between P' and the emitting cylinder is an ellipse which is straightforwardly parameterised by ρ, ϕ, and an polar angle ξ measured in the plane P. The geometric disposition of these planes and angles is illustrated in Fig. 3. The observed intensity is then obtained by integrating the projection of the local intensity field onto the line of sight and integrating over the emitting regions within the observers field of view.

The surface accessible to the observer depends on the viewing angle. Consider first the pole labelled **North** in Fig. 2. If ϕ is such that the point $Z_1 > h$, then the north cylinder is completely hidden from view, therefore $I = 0$ at this pole. When $Z_1 < h$, two cases arise depending on the value of $Z_0 = R(1-\cos\phi)/\cos\phi$, i.e. the point of intersection between the line of sight and the magnetic axis. Posing z_0 such that $Z_0 = z_0 R$, integration over the observable surface of the north cylinder yields, case 1. ($z_0 < y$):

$$I = 4\pi E_0 x R^2 \cos\phi \left(y - z_0 + \frac{\pi^2 x}{2} \tan\phi \right), \qquad (1)$$

and, case 2. ($z_0 > y$):

$$I = 4\pi E_0 x R^2 \cos\phi \left[(y - z_0)\cos\xi_0 + \pi x \tan\phi \left(\frac{\pi}{2} - \xi_0 + \frac{\sin 2\xi_0}{2} \right) \right]. \qquad (2)$$

Where the angle $\xi_0 = \arcsin[(z_0 - y)/(2\pi x \tan\phi)]$.

Note that a when $\sin\phi < 2\pi x$, or equivalently when the point, T, where the line of sight is tangent to the surface of the neutron star is situated within the cylinder wall, Eqs. (1) and (2) are incomplete (see Fig. 2) and must be supplemented by,

$$I = 4\pi E_0 x R^2 \cos\phi \left[(y - z_0)\cos\xi_0 + \pi x \tan\phi \left(\frac{\pi}{2} - \xi_0 \frac{\sin 2\xi_0}{2} \right) + \frac{\kappa'^2}{2\kappa} \ln(\sqrt{1-\kappa^2}) - \frac{\Delta\cos\xi_0}{2} - \frac{\kappa'^2}{2\kappa} \ln(\kappa\cos\xi_0 + \Delta) \right], \qquad (3)$$

the integration over that part of the cylinder below the plane P' still within the observer's field of view. In Eq. (3) the angle $\xi_0 = \arcsin[\sin\phi/(2\pi x)]$, $\kappa = 2\pi x$, $\kappa'^2 = 1 - \kappa^2$, and $\Delta^2 = 1 - \kappa^2 \sin^2\xi_0$.

Consider now the pole labelled **South** in Fig. 2. Half the cylinder is observed at an angle ϕ. For this pole,

$$I = 4\pi E_0 x R^2 \cos\phi \left[\frac{1}{2} + \frac{\kappa'^2}{2\kappa} \ln(\sqrt{1-\kappa^2}) - \frac{\kappa'^2}{2\kappa} \ln(1+\kappa) + y \right]. \qquad (4)$$

The intensity reaching the observer is the sum of the emission from the surface of the walls of each cylinder within his field of view . The angle ϕ is modulated by the rotation of the neutron star. Introducing the angles θ_m, between the rotation axis and magnetic axis, and θ_r between the rotation axis and the line of sight, the viewing angle θ to the north magnetic pole can be determined using the equation from Smart (1965),

$$\cos\theta = \cos\theta_r \cos\theta_m + \sin\theta_r \sin\theta_m \cos\Phi, \qquad (5)$$

as a function of the neutron star's pulse phase, Φ. The angle of interest here, namely ϕ, is simply such that $\theta = \pi/2 + \phi$. Note that Eqs. (1) to (4) hold only if $\phi \geq 0$, in the contrary case, the axial symmetry of the system implies that the poles are interchanged. Thus by replacing ϕ by $-\phi$, and inverting the poles, the same equations are in fact valid.

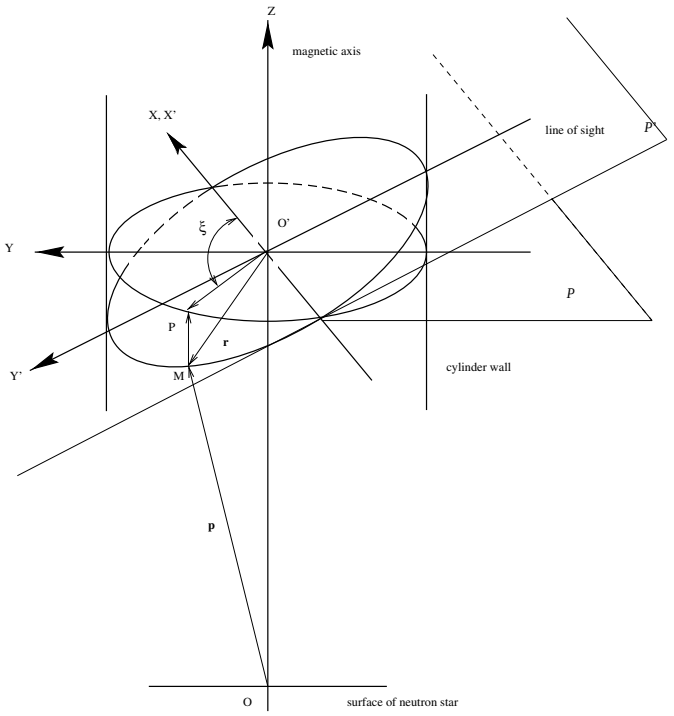

Fig. 3. The detailed geometry of the cylinders showing the definition of the angles and reference coordinate systems used to parameterise the emitting cylinders. The reference frame XO′Y is in the plane P perpendicular to the magnetic axis Z, X′O′Y′ is in plane P'.

We must emphasise here that the models used to determine the inclinations between the magnetic axis and the line of sight relative to the rotation axis may have a large impact on their deduced values. To grasp this more clearly consider the present model with only one cylinder, in the limiting case where $\theta_r = \theta_m = \pi/2$. Let the origin of the phase angle Φ be at that moment when the magnetic axis is perpendicular to the line of sight. In this configuration, the observed emission begins to rise from zero when the top of the cylinder first crosses the line of sight, viz. when $\Phi_1 = -\arccos(1/1+y)$. The observed intensity then rises more or less rapidly to maximum at $\Phi = 0$ and will decrease to zero at $\Phi = \pi/2$, when the line of sight is parallel to the stellar magnetic axis. From $\pi/2$ to $\pi + \Phi_1$ the profile is mirror symmetric. Between $-\Phi_1$ and $\pi + \Phi_1$ the cylinder is no longer visible to the observer since it is behind the neutron star. Therefore, in the present model, there exist configurations for which only one pole will yield a twin peaked profile. Contrarily, for the same values of θ_r and θ_m, a single polar cap model will produce only one peak with a maximum of observed emission at $\Phi = \pi/2$. In fact, in a polar cap/ring model, two polar caps/rings are required in order to produce two distinct peaks in the light curves.

More generally, three cases occur for our model.

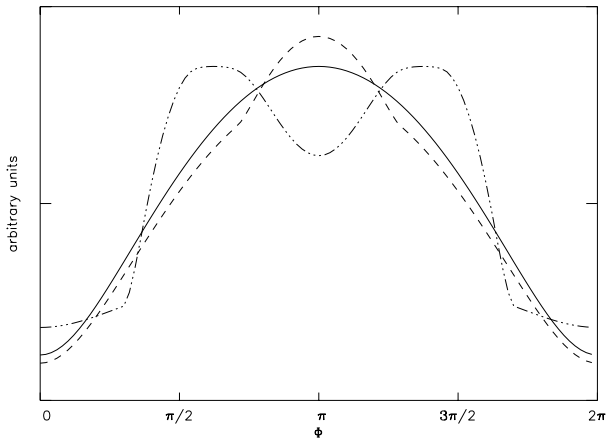

Fig. 4. Example of pulse profiles obtained with the model. The parameter $x = 0.015$ for all curves. Case 1 (see text), solid line, $y = 0.05$, $\theta_m = 20°$, $\theta_r = 10°$. Case 2, dashed line, $y = 1$, $\theta_m = 20°$, $\theta_r = 10°$. Case 3, dashed–dotted line, $y = 0.05$, $\theta_m = 25°$, $\theta_r = 80°$. See text for a discussion on the possible forms of the pulse profiles.

1. $\theta_r + \theta_m < \pi/2$, depending on the value of x and y, the observer sees only one peak, one of the poles always remains completely hidden from view,
2. $\theta_r + \theta_m < \pi/2$, but x and y are such that the observer sees the sum of the contributions from both poles, both poles will cross into the observer's field of view in the course of one revolution of the neutron star,
3. $\theta_r + \theta_m > \pi/2$, in which case both poles will also be visible, the magnetic axis crosses the plane perpendicular to the line of sight.

When $\theta_r + \theta_m < \pi/2$, the condition on x and y for both poles to be in the field of view of the observer is written as,

$$y > \frac{1}{\sin(\theta_r + \theta_m)} \left[1 - 2\pi x \cos(\theta_r + \theta_m) \right] - 1.$$

It should be also noted that, for some configurations of θ_r and θ_m, in which y is sufficiently high, i.e. a part of the cylinder is always visible to the observer, the minimum value of the intensity reaching the observer never becomes zero. In these cases, the impression of a steady component, emitted by the cylinder, appears in the light curves. Examples of the profiles obtained for these three cases are shown in Fig. 4.

4. Fitting the γ–ray light curves of GX 1+4

The model described above is completely determined by five parameters, namely E_0, θ_r, θ_m, x and y. With the exception of E_0, these parameters describe the geometric configuration of the system. However, the data in itself offers no clue as to the values which these parameters might take. Furthermore, for a given pulse profile, a unique decomposition into two symmetric functions defining the emission from each of the poles is not always possible. This is shown by Kraus et al. (1995) in the general case where the pulse profile is asymmetric. Following their reasoning, this indeterminacy is inherent when the pulse profile is symmetric. Moreover Eqs. (1) to (4) are also highly nonlinear, far from simplifying any fitting procedure.

The observed light curves are in some instances notably asymmetric while, by construction, the theoretical profiles which result from Eqs. (1)–(4) are mirror symmetric. The SIGMA data however exhibits somewhat large uncertainties. Rather than attempting to introduce asymmetries into the model via still other parameters at this stage, we chose instead to symmetrize the profiles before fitting. To achieve this in an objective way, the binned light curves were first symmetrized relative to each bin. The resulting profile which minimised $\chi^2 = \sum (Y_i - S_i)^2$, where Y_i and S_i are the original and symmetrized data in the i^{th} phase bin, was employed in the analysis. The distributions of the count rates are then obtained by subtracting the background and adding the steady flux component to the profiles. The steady flux component, S, obtained from the image data, is taken as the count rate at the pixel corresponding to the SIGMA position of GX 1+4. The distribution obtained from the actual data is thus written as $S_d = Y_i - (\sup[Y_i] + \inf[Y_i])/2 + S$ while that which is actually fitted is $S_f = S_i - (\sup[S_i] + \inf[S_i])/2 + S$.

To justify this attitude we note that in a comparison between the symmetrized and original count rate distributions, the Kolmogoroff–Smirnov test showed that both distributions are in fact compatible with the same parent distribution to within a 95% confidence level. In other words, from a statistical point of view, we commit a minimal degradation of the original data by symmetrizing the pulse profiles. Three exceptions occur, the observations on JD_m 9232, JD_m 9233, and JD_m 9249. For these three observations, however, no spectral data was available. It should be noted that the difficulty in correctly determining the steady flux component may influence the count rate distribution. Furthermore, $\inf[Y_i]$ and $\inf[S_i]$ differ in general. This is probably responsible for discrepancies between the two distributions.

A final assumption in determining acceptable fits is imposed on the dimensions of the accretion column. This is, to a certain degree, of a pragmatic nature since the values of the height and width of the accretion funnel can not be inferred from the data. Furthermore, the parameters E_0, x, and y are not strictly speaking fully independent. This can be understood on physical grounds. Note, that xy is proportional to the surface of the cylinder and since E_0 is a measure of the specific intensity, it is inversely proportional to xy.

According to Basko & Sunyaev (1976), the height of the accretion column, defined as the position of the shock zone above which high energy emission is absent, depends on the mass accretion rate. For low accretion rates, they estimate $\rho \sim 0.1R$ (or $x \sim 0.015$) and $h \sim 0.005R$ (or equivalently $y \sim 0.005$). For high accretion rates, the shock zone may be well above the stellar surface, even reaching the Alfén radius. For GX 1+4 there is no indication that the accretion rate is overly high, also the mass losing companion of the neutron star is

Table 3. Values of the parameter y

JD_m	y ($\times 10^{-3}$)	χ^2_ν	JD_m	y ($\times 10^{-3}$)	χ^2_ν
8671	5 ± 1	0.11	9971	9 ± 1	0.14
9232†	1 ± 1	0.38	9978	3 ± 1	0.70
9233†	no fit		9979†	1 ± 1	0.39
9236	5‡	0.08	10162	3 ± 1	0.12
9238	3 ± 1	0.06	10164	4 ± 1	0.20
9242	4 ± 1	0.09	10167	2 ± 2	1.85
9244	6 ± 2	0.09	10168†	4 ± 2	0.50
9246	0.4 ± 0.4	0.23	10172†	1 ± 2	1.00
9249†	no fit				

‡, the observation 9236 was used to obtain the values of $\theta_m \sim 84°$ and $\theta_r \sim 5°$, y = 0.005 and x = 0.015. For all other fits θ_m, θ_r, were held constant along with x = 0.015. On dates flagged with a †, no spectrum was available. For all fits the number of degrees of freedom is 8 except for JD_m 9236 with 7 d.o.f.

an M type giant, which, although it probably presents erratic behaviour in its mass outflow, is not expected to be in a high mass loss regime. We thus tacitally assume that GX 1+4 has a low accretion rate and impose the corresponding values of x and y and, proceed to fit for the values of θ_m and θ_r for the observation JD_m 9236 which is taken as reference since the S/N ratio on this date was relatively high but this choice is somewhat arbitrary.

For this observation these angles are found to be $83.57° \pm 0.34°$ and $4.60° \pm 0.34°$. Because Eq. (5) is symmetric with respect to θ_m and θ_r, we can not decide which value is assigned to which angle. It is unlikely that these angles vary much on the time scale of six years unless the system suffered some catastrophic event. Thus, for all other observations, θ_m and θ_r were held fixed along with x. Only y and E_0 need to be fitted. The resulting values of y are listed in Table 3. Uncertainties in the parameter y were calculated using the covariance matrix for which we have used the product $2J^TJ$, where J is the Jacobian matrix, to approximate the Hessian matrix.

5. Discussion and conclusion

At the time of its first detection, GX 1+4 was in a high state which persisted from 1971 to about 1980. The source entered into a low state initiated between 1980 and 1981 when the pulsar underwent a torque reversal and commenced its present day spin–down episode. Since then, the general trend in its X–ray luminosity been a relatively low state. although, GX 1+4 has experienced a number of X–ray flares on shorter time scales (see e.g. Chakrabarty et al. 1996, Manchanda et al. 1995). Flaring activity is not apparent in the SIGMA data. During the last four years, to within errors, the X–ray luminosity of GX 1+4 has been generally close to the mean value of $\sim 5.46\ 10^{36}$ erg $^{-1}$ cm^{-2} similar to its 1991 March/April value (Laurent et al. 1993). The mean spectral index was found to be $-3.25^{+1.1}_{-1.6}$.

From 1970 to circa 1980 GX 1+4 was in a spin–up phase during which the rotational period steadily decreased from $\sim$ 138 s (Lewin et al. 1971) to $\sim$ 110 s (Ricketts et al. 1982) at a rate of ~ -2.7 s yr^{-1}. In 1986 November the pulsation period was reported to be $\sim$ 111 s (Greenhill et al. 1993). Observations accumulated thereafter have provided clear evidence that the pulsar had entered into a spin–down phase sometime between 1980 and 1986. Although fluctuations in the spin–down behaviour of the neutron star have been noted (e.g. Chakrabarty et al. 1994, Chakrabarty et al. 1995, Laurent 1995), the general trend of the prolonged spin–down episode still continues. This behaviour is confirmed by the SIGMA observations.

The periods obtained by SIGMA in the soft γ–ray band from 1992 onward are compatible with those found by other instruments operating in other energy ranges, e.g. BATSE, X–ray balloon observations, and even a recently recorded pulsation period of 124.17 s in the U band from its optical counterpart V2116 Oph (Jablonski et al. 1996),presumably linked to the the high energy emission from the neutron star. A value of $\dot{P}$ can be inferred by fitting a line to the SIGMA data points. $\dot{P}$ varies from one month to another, the average period derivative is 1.35 ± 0.06 s yr^{-1}.

Modelling of the pulse profiles provides insight into the geometries and beam patterns which can be associated with accretion powered binary pulsars. For the source GX 1+4, a few determinations of the angles θ_m and θ_r are available from the literature. A widely used model for the emission regions is a filled polar cap or ring situated at the magnetic pole. Assuming this geometry, dipole symmetry, and the calculated radiation distribution obtained under the assumption of an emitting slab (Mészáros & Nagel 1985), Leahy (1990) finds the values of $\sim 82.5°$ and $\sim 14.9°$. In (1991) the same author, after introducing deviation from dipole symmetry by including an offset angle between the poles, found θ_m to be $\sim 83°$, a value very close to what is found with our model and nearly equal to that found in his first study. For θ_r the values given are $\sim$ 14.9 and $\sim 6.9°$ depending on whether the observed flux is written as a function of $\cos^2\ \theta$ or $\cos^4\ \theta$ (refer to Leahy 1990 for a discussion). There is some ambiguity however as to which decomposition of the observed flux is more appropriate. The offset angle is given to be 6°, but Leahy also points out in this last study that the pulsar GX 1+4 can be acceptably fitted with the two identical polar cap model without the need of an offset angle.

Li & Wang (1992) calculate θ_m to be $\sim 33.6°$ or $\sim 27°$ depending on whether the pulsar is spinning up or down. Their calculation is based on other considerations, mainly on accretion disk models and requires a accurate determination of the X–ray luminosity. However, disk accretion models are built around numerous simplifying assumptions and the discrepancy between the different values may be due to these as well as to the quality of the data. A more recent result, which is in net discord with ours, is from Paul et al. (1997) who find $\theta_m = \theta_r = 56° \pm 8°$. This value is obtained for a polar cap model, assuming a simple fan beam pattern, a symmetric dipole with equal intensity on both sides of the equator. From the above reported values, it is clear that the determinations of the angles are model dependent and is not as straightforward as one might hope.

A careful examination of the pulse profiles depicted in Fig. 1 reveals differences from one observation to another although these should be considered qualitive in light of the poor data. For example, on JD_m 9233 and JD_m 9244 a dip might be present in the pulse profile which is less evident on JD_m 8671. The apparent asymmetry on JD_m 9246 and JD_m 9249 is much less prominent, even reversed, on JD_m 8671. Subtle differences may be enhanced or smoothed depending on binning. Statistically, however, we can catagorize the profiles by submitting the data to the Kolmogoroff–Smirnov test.

To within a 95% confidence level, the observations for which a pulse profile could be extracted, and for which the corresponding image data independently provided a spectrum above a S/N ratio of 3σ, roughly fall into one class. Denote this class as C_1. Only the observations on JD_m 9246 and JD_m 10167 escape clear classification although on these dates there are no appreciable peculiarities in the SIGMA data. On the other instances when GX 1+4 was below the detection threshold in the images, the Kolmogoroff–Smirnov test is inconclusive. Observations pertaining to these dates being compatible with few others or altogether incompatible with all others. We group these observations into class C_2. These classes appear to be linked to the pulsed fractions, C_1 contains those observations with a pulsed fraction less than $\sim$ 50%, and C_2 includes those with a pulsed fraction greater than $\sim$ 50%. The ambiguous case on JD_m 9246 could be included into the class C_2 since on this date the pulsed fraction is 79%. The observation on JD_m 10167 must be a limiting case since on this occasion the pulsed fraction is 48%.

The class C_1 has an average y, $\bar{y} \sim (5 \pm 1) \times 10^{-3}$. Only the observation on JD_m 9971 presents a high value of the height of the accretion column. On this date there is no notable event in the SIGMA data. For C_2, $\bar{y} \sim (2 \pm 2) \times 10^{-3}$. Because of the lack of observations and the uncertainties involved in the data, we tentatively propose the conclusion that a low accretion column produces high pulsed fractions. This is compatible with the model predictions, since a higher accretion column will not fully disappear from the observers field of view; the higher the column the greater the importance of the steady flux component. For the observations where no spectrum could be extracted from the data, the accretion column tends to have a lower height or the model is unable to fit the data, generally because y approaches zero and the model equations break down. However, only two observations could not be fitted, namely on JD_m 9233 and JD_m 9249. Our model is not completely adequate to describe all of the data, at least in its present formulation. We note in passing that a filled accretion column might occur at times for GX 1+4, as suggested by Dotani et al. (1989) to explain the peculiar profiles obtained by GINGA. They propose that a hollow column is the case when a dip in the pulse profile is seen while a filled column produces a profile in which this dip is absent.

The angles reported in Sect. 4 do not yield a pulse profile with a double peaked structure whatever the values of y. In fact, a double peaked pulse profile requires angles which fulfil the condition $\theta_r + \theta_m > \pi/2$. However, we find it possible to fit some of the observations with angles that meet the above constraint. For example, $\theta_m \sim 26°$, a value close to that proposed by Li & Wang (1992), and $\theta_r \sim 78°$ will result in very acceptable fits to the observations on JD_m 8671 and JD_m 9971. However, fits to other observations are more difficult precisely because these values for the angles produce a dip in the light curves. We can improve the model presented here by considering the geometry of a filled accretion column. In this case, the presence or absence of a dip can be modelled, but this is left to a future paper in which an eventual modelling of the asymmetry of the profiles will also be included. For this, however, we are in need of higher quality data and long term monitoring of more accretion powered pulsars in order to elaborate the pulsar emission model. It is hoped that the next generation of γ–ray observatories will provide this data.

References

Barret D., Mereghetti S., Natalucci L., et al., 1991, in: Durouchoux P., Prantzos N. (eds), Proc. Internat. Symp. on Gamma–Ray Line Astrophysics, Saclay, AIP Conf. Proc. 232, New York, p. 42

Basko M.M, Sunyaev R.A., 1976, MNRAS, 175, 395

Chakrabarty D., Finger M. H., Prince T.A., 1996, IAUC 6478

Chakrabarty D., Koh T., Prince T. A., et al., 1995, IAUC 6153

Chakrabarty D., Prince T. A., Finger M. H., et al., 1994, IAUC 6105

Davidsen A., Malina R., Bowyer S., 1977, ApJ, 211, 866

Davidsen A., Malina R., Bowyer S., 1976, ApJ, 203, 448

Dotani T., Kii T., Nagase F., et al., 1989, PASJ, 41, 427

Goldwurm A., 1996, Experim. Astron., 6, 9

Greenhill J. G., Sharma D. P., Dieters S. W. B., et al., 1993, MNRAS, 260, 21

Jablonski F., Pereira M., Braga J., et al., 1996, IAUC 6489

Kraus U., Nollert H.-P., Rudder H., Riffert H., 1995, ApJ, 450, 763

Laurent P., 1995, in: Alpar M.A. (ed), The Lives of Neutron Stars, Kluwer Academic Publishers, Netherlands, p. 405

Laurent P., Salotti L., Paul J., et al., 1993, A&A, 278, 444

Leahy D.A., 1991, MNRAS, 251, 203

Leahy D.A., 1990, MNRAS, 242, 188

Leahy D. A., Darbro W., Elsner R. F., Weisskopf M. C., 1983, ApJ, 266, 160

Lewin W. H. G., Ricker G. R., McClintock J. E., 1971, ApJ, L17

Li X.-D., Wang Z.-R., Comments Astrophys., 1992, Vol. 16, No. 4., 219

Manchanda R.K., James S.D., Lawson W.A., et al.: 1995, A&A, 293, L29

Mésáros P., Nagel W., 1985, ApJ, 299, 183

Mukai K., 1988, 1984 Low State of GX 1+4, Mullard Space Laboratry internal report

Makishima K., Ohashi T., Sakao T., et al., 1988, Nat., 333, 746

Paul B., Agrawal P.C., Rao A.R., Manchanda R.K., 1997, A&A, 319, 507

Paul J., Mandrou P., Ballet J., et al., 1991, Adv. Space Res., 11 (8), 289

Ricketts M. J., Hall R., Page C., et al., 1982, MNRAS, 201, 759

Smart W.M, 1965, Text–book on Spherical Astronomy, pp. 6–10, Cambridge University Press, London

This article was processed by the author using Springer-Verlag LaTeX A&A style file *L-AA* version 3.